Journal of the Indian Chemical Society 101 (2024) 101275

Contents lists available at ScienceDirect

Journal of the Indian Chemical Society

journal homepage: www.journals.elsevier.com/journal-of-the-indian-chemical-society

Exploration of supramolecular interactions, Hirshfeld surface, FMO, molecular electrostatic potential (MEP) analyses of pyrazole based Zn (II) complex

Suranjana Chatterjee [a], Mohd Afzal [b], Pulak Chandra Mandal [c], Ritwik Modak [d], Mridula Guin [e,*], Saugata Konar [f,**]

[a] Department of Chemistry, Ananda Mohan College, Kolkata, 700009, India
[b] Department of Chemistry, College of Science, King Saud University, Riyadh, 11451, Saudi Arabia
[c] Department of Chemistry, Raja Rammohun Roy Mahavidyalaya, Hooghly, 712406, India
[d] Department of Chemistry, Manipal Institute of Technology Bengaluru, Manipal Academy of Higher Education, Manipal, 576104, India
[e] Department of Chemistry and Biochemistry, Sharda University, Greater Noida, Uttar Pradesh, 201310, India
[f] Department of Chemistry, The Bhawanipur Education Society College, Kolkata, 700020, India

ARTICLE INFO

Keywords:
Supramolecular interactions
MEP
HOMO and LUMO
Hirshfeld surface

ABSTRACT

The supramolecular interactions of title compound $[Zn(HL_2)](ClO_4)_2(MeOH)_2$ (**1**) where, HL_2=((Z)-N'-(5-methyl-1H-pyrazole-3-carbonyl)pyrazine-2-carbohydrazonamide) are explored in detail. With a detailed scrutiny of visualizing of title compound **1,** the crystal packing is mainly directed by strong hydrogen bonding interactions observed N–H···N and N–H···O but, in addition, weak interactions such as C–H···π, π···π are also sighted to stabilize the crystal self-assembly. Electronic structure of the complex is determined using DFT calculations at B3LYP level with mixed basis set. Theoretically calculated structural parameters are in good match with the experimentally obtained parameters from XRD. TDDFT calculation is performed to simulate the UV–Vis absorption spectra of the complex. Molecular reactivity and stability of the complex has been assessed through frontier molecular orbital analysis and also through evaluation of molecular electrostatic potential (MEP). Hirshfeld surface analysis, which uses molecular surface contours and 2D fingerprint plots to visually analyze intermolecular interactions in crystal structures, has been used to examine molecular morphologies. The Hirshfeld surface and fingerprint plots are accompanied by crystal structure analysis allowed for the discovery of the important intermolecular interactions.

1. Introduction

The pyrazole-based chelating ligands have received a lot of attention in coordination chemistry [1,2]. The polydentate ligands based on pyrazoles exhibit preparative accessibility, structural variation, and varying denticity, generating complexes with various nuclearities and coordination numbers and with intriguing molecular topologies. The literature has seen a lot of research on iminopyrazine-2-carboxylic acid (or, iminopicolinic acid) ligands produced from pyrazoles, but less on computational studies as well as Hirshfeld surface analysis. It is generally known that one of the crucial elements in the investigation of crystal engineering is the careful selection of the organic ligands.

Moreover, supramolecular frameworks coupled by intermolecular interactions continue to be a key topic in solid-state investigations of "self-assembly" when it comes to crystal engineering [3,4]. The basic objective of crystal engineering is to manage the topology of crystal packing for functional solids through covalent and non-covalent interactions, since a successful inclusion of suitable structural units into a crystal may lead to the production of innovative materials [5]. Although hydrogen bonds continue to be the most effective and common way to enforce molecular recognition of crystalline materials, other, weaker forces like the π-π forces connected to aromatic-π systems have also been successfully applied in this context.

Furthermore, the global scientific community respects and uses the

* Corresponding author.
** Corresponding author.
E-mail addresses: mridula.guin@sharda.ac.in (M. Guin), saugata.konar@gmail.com (S. Konar).

https://doi.org/10.1016/j.jics.2024.101275
Received 25 February 2024; Received in revised form 21 June 2024; Accepted 20 July 2024
Available online 23 July 2024

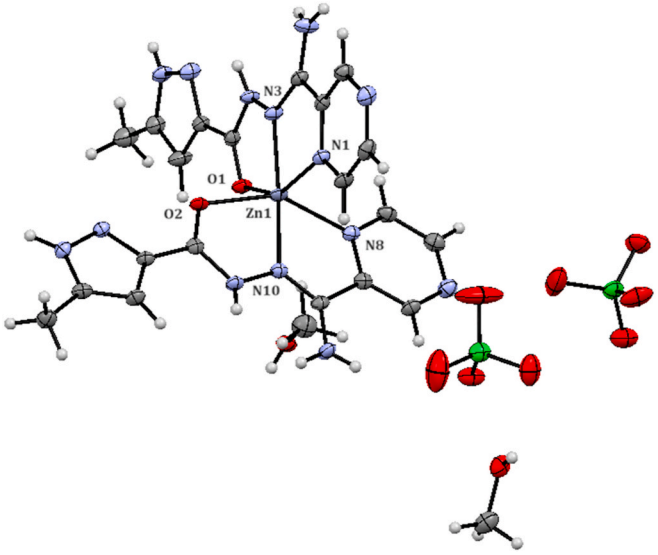

Fig. 1. ORTEP diagram (50 % ellipsoid probability) of **1**.

density functional theory (DFT) technique for predicting the electronic structures of transition metal complexes [6,7]. It supports interpretation and elucidation of molecular structure and characteristics. The energy difference between HOMO and LUMO is used to calculate a number of parameters that are crucial to understanding a compound's potential for use in the biomedical field and other applications. Additionally, a crucial indicator of a compound's polarity and reactivity is its molecular electrostatic potential (MEP). In terms of hydrogen bonds, enzyme-substrate interactions, or drug-receptor interactions, MEP may precisely identify a wide variety of molecular interactions. By using surface contours in terms of d_{norm}, shape index, and curvature, molecular Hirshfeld surface analysis [8] aids in visualizing intermolecular interactions and packing modes of a crystal. Fingerprint plots in two dimensions are used to assess the contributions of different near contacts in crystal packing.

As part of our ongoing studies [9], we have elucidated the weak interactions in between aromatic π-ring of the solid state. Non-covalent interactions such as π … π and CH … π are crucial for forming an extensive network in the synthesized metal complex framework. An investigation of close intermolecular contacts between the molecules *via* Hirshfeld surface analysis is also presented in order to reveal subtle differences and similarities of metal complex in the crystal structure. Additionally, the title compound's molecular electrostatic potential (MEP) and frontier molecular orbitals (FMO) are further examined by DFT, providing details about its molecular structure and conformations.

2. Experimental

2.1. Density functional theory (DFT) study

All quantum chemical calculations are performed using Gaussian 16 program package [10]. The ground state geometry of the complex was determined using DFT calculation by B3LYP functional with mixed basis set. 6-31 + G* basis set was used for all atoms except zinc for which effective core potential LANL2DZ basis set was utilized. The hybrid B3LYP functional along with LANL2DZ basis set for transition metal complexes is known to provide best result in predicting geometrical parameters with limited computational cost. The counter ions methanol and perchlroate ions are omitted during structural optimization. The convergence criteria were maintained at default level without any constraint on the geometry. The visualization of the electronic structure was performed using Gaussview 6.0 program. The frequency calculation does not produce any negative frequency and thereby confirming the

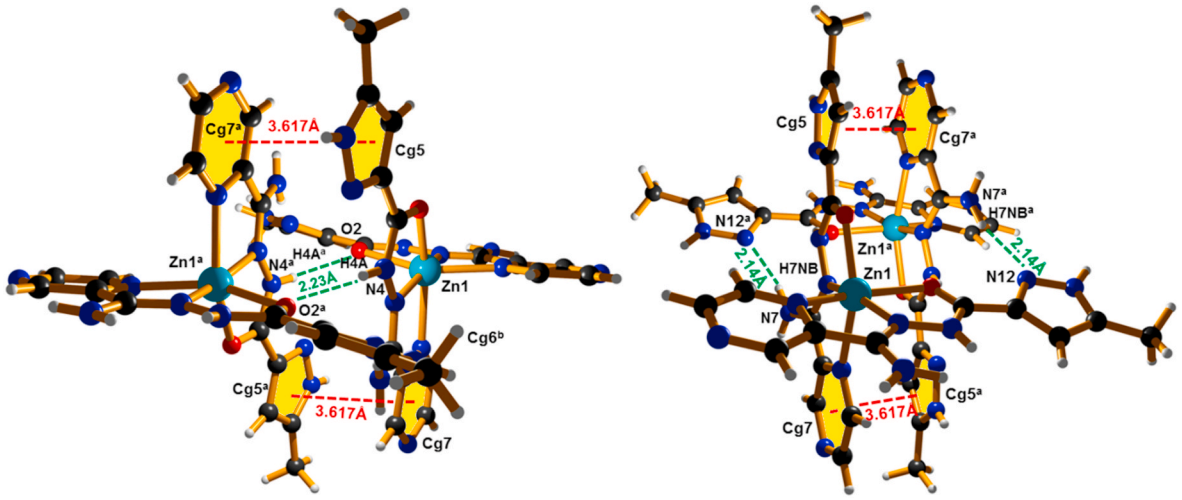

Fig. 2. Formation of dimeric unit with intra-molecular hydrogen bonds and π···π stacking interaction (where dotted green lines and dotted red lines respectively represent Hydrogen bonding and π···π interaction). [Symmetry transformation for equivalent atoms: ([a]) –x, –y,–z]

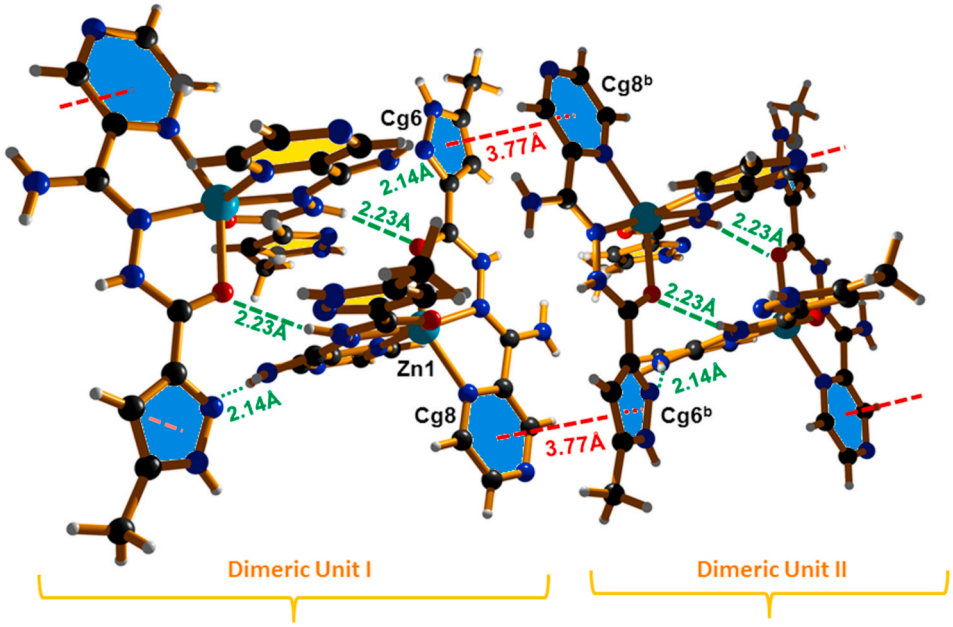

Fig. 3. Formation of 1D Chain through inter-molecular π···π stacking interaction interactions (shown as dotted red lines). [Symmetry transformation for equivalent atoms: (^{b}) = 1–x, –y, –z]

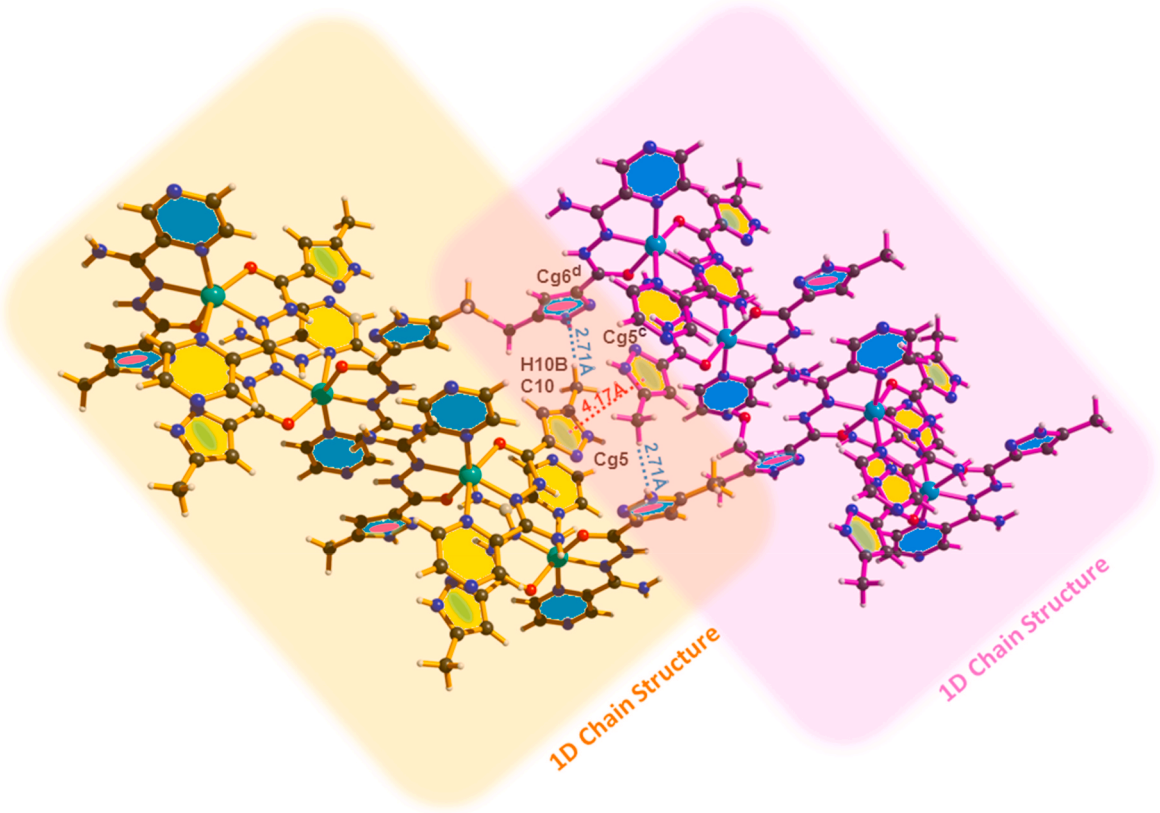

Fig. 4. Formation of 2D sheet like network through intermolecular π···π stacking and C–H···π interaction interactions (shown as dotted red and blue lines respectively). [Symmetry transformation for equivalent atoms: (^{c}) = –X,1–Y,–Z and (^{d}) = X, 1 + Y, Z]

optimized geometry as true minima on the potential energy surface. Energy of HOMO (Highest Occupied Molecular Orbital), LUMO (Lowest Unoccupied Molecular Orbital) and band gap is determined to understand the chemical reactivity of the compound. Moreover, molecular electrostatic potential of the compound is calculated from the electron density to predict the electrophilic and nucleophilic regions in the complex.

Table 1
Selected bond lengths and bond angles of Complex **1**.

Selected bonds	Bond lengths (Å)		Bond angles	Bond angles (°)	
	XRD	DFT		XRD	DFT
Zn1–O2	2.1375 (17)	2.333	N6–Zn1–N17	162.72(8)	175.32
Zn1–O3	2.1833 (18)	2.298	N6–Zn1–O2	76.13 (7)	71.42
Zn1–N17	2.032 (2)	2.111	N6–Zn1–O2	96.06 (7)	103.54
Zn1–N15	2.258 (2)	2.197	N6–Zn1–N15	115.77 (8)	109.52
Zn1–N4	2.168 (2)	2.217	N17–Zn1–O2	117.68(7)	106.97
Zn1–N6	2.050 (2)	2.123	N17–Zn1–N15	75.34(8)	74.92
O2–C34	1.249 (3)	1.250	O2–Zn1–N15	94.15 (7)	96.96
O3–C51	1.247 (3)	1.249	N17–Zn1–O3	74.53 (7)	71.88
N4–C26	1.339 (3)	1.341	O2–Zn1–O3	90.46 (7)	88.04
N4–C32	1.347 (3)	1.387	N15–Zn1–O3	148.03 (7)	146.43
N5–C28	1.330 (3)	1.365	N6–Zn1–N4	74.01 (7)	74.14
N5–C30	1.348 (3)	1.321	N17–Zn–N4	92.65 (8)	107.27
N6–C33	1.298 (3)	1.324	O2–Zn1–N4	149.67 (7)	145.56
N6–N7	1.388 (3)	1.362	N15–Zn1–N4	94.03(8)	95.21
N7–C34	1.341 (3)	1.365	O3–Zn1–N4	97.78 (7)	99.17
N9–C35	1.337 (3)	1.341	C34–O2–Zn1	112.95(15)	111.74
N9–N10	1.346 (3)	1.346	C51–O3–Zn1	113.35(16)	113.02
N10–C38	1.348 (3)	1.368	C26–N4–C32	116.7(2)	116.46
N12–C33	1.321 (3)	1.405	C26–N4–Zn1	130.34(17)	129.32
N15–C43	1.332 (3)	1.343	C32–N4–Zn1	112.95 (16)	113.75
N15–C49	1.351 (3)	1.393	C28–N5–C30	117.1(2)	116.10
N16–C45	1.326 (3)	1.369	C33–N6–N7	120.1 (2)	120.99
N16–C47	1.342 (3)	1.319	C33–N6–Zn1	123.69(17)	120.19
N17–C50	1.293 (3)	1.333	N7–N6–Zn1	114.95(15)	117.98
N17–N18	1.380 (3)	1.362	C34–N7–N6	114.3(2)	115.87
N18–C51	1.350 (3)	1.371	C35–N9–N10	103.2 (2)	104.08
N20–C52	1.339 (3)	1.338	N9–N10–C38	113.9 (2)	113.77
N20–N21	1.345 (3)	1.346	C43–N15–C49	117.0 (2)	116.33
N21–C55	1.363 (3)	1.366	C43–N15–Zn1	129.03 (17)	130.01
N23–C50	1.326 (3)	1.417	C49–N15–Zn1	113.75 (17)	113.45
C26–C28	1.389 (4)	1.387	C45–N16–C47	123.7(4)	116.16
C30–C32	1.375 (4)	1.416	C50–N17–N18	121.9(2)	120.59
C32–C33	1.501(3)	1.436	C50–N17–Zn1	121.78(18)	119.34
C34–C35	1.465(3)	1.469	N18–N17–Zn1	116.13(16)	117.80
C35–C36	1.397 (4)	1.417	C51– N18–N17	114.4(2)	115.77
C36–C38	1.372(4)	1.383	C52–N20–N21	104.2(2)	104.21
C38–C39	1.495 (4)	1.497	N20–N21–C55	112.6(2)	114.20
C43–C45	1.395 (4)	1.385	N4–C26–C28	121.8(2)	122.73
C47–C49	1.382 (4)	1.421	N5–C28–C26	121.3 (2)	121.66
C49–C50	1.502 (3)	1.425	N5–C30–C32	121.7(2)	123.78
C51–C52	1.468 (3)	1.472	N4–C32–C30	121.4(2)	119.17
C52–C53	1.406 (3)	1.426	N4–C32–C33	115.1(2)	116.16
C53–C55	1.367(4)	1.382	C30–C32–C33	123.5(2)	124.65
C55–C56	1.493(4)	1.497	N6–C33–N12	127.3(2)	120.54
			N6–C33–C32	119.8(2)	115.20
			O2–C34–N7	121.2 (2)	120.80
			O2–C34–C35	121.7 (2)	122.84
			N4–C34–C35	117.0 (2)	116.35
			N9–C35–C36	112.0 (2)	111.54
			N9–C35–C34	119.9 (2)	121.46
			C36–C35–C34	128.1 (2)	127.00
			C38–C36–C35	105.2 (2)	105.18
			N10–C38–C36	105.6 (2)	105.42
			N10–C38–C39	122.8 (2)	122.62
			C36–C38–C39	131.6 (3)	131.95
			N15–C43–C45	121.1 (2)	122.96
			N16–C45–C43	122.3 (2)	121.59
			N16–C47–C49	121.9 (2)	123.94
			N15–C49–C47	121.2 (2)	118.92
			N15–C49–C50	115.3 (2)	116.38
			C47–C49–C50	123.5 (2)	124.68
			N17–C50–N23	127.7 (3)	119.58
			N17–C50– C49	112.7 (2)	115.32
			N23–C50– C49	119.5 (2)	125.04
			O3–C51–N18	120.8 (2)	119.97
			O3–C51–C52	122.2 (2)	124.14
			N18–C51– C52	117.0 (2)	115.87
			N20–C52– C53	111.7 (2)	111.03
			N20–C52– C53	116.8 (2)	119.94
			C53–C52– C51	131.5 (2)	129.02
			C55–C53– C52	104.9 (2)	105.46
			N21–C55– C53	106.6(2)	105.08
			N21–C55– C56	121.5 (2)	122.92
			C53–C55– C56	131.8(2)	131.99

2.2. Molecular Hirshfeld surface analysis

Hirshfeld surface analysis is widely used tool for understanding the intermolecular interactions in a molecular crystal. The intermolecular close contacts can be visualized qualitatively and quantitatively through the Hirshfeld surface. The red-white-blue colour surface of the normalized contact distance *d*norm identifies the close contacts around van der Waals radius, short contacts and long contacts. The mapped *d*norm surface shows red spots wherever close contacts are present in the molecular crystal.

Crystal Explorer 17.5 program [11] is used to perform Hirshfeld surface (HS) analysis of the complex using the cif file. Three colour coded surface e.g., *d*norm, shape index and curvedness were mapped for the molecular crystal. The Hirshfeld surface was generated using a high standard surface resolution. All the surfaces were presented in a transparent mode for clear visualization. Additionally, 2D fingerprint plots in terms of d_e and d_i are determined to summarize the nature and type of intermolecular contacts used in packing of the molecular crystal.

3. Results and discussion

3.1. Supramolecular features

The molecular structure is presented in Fig. 1. The hydrogen bonding interactions form 2D array of supramolecular network with the help of perchlorate anion and solvent molecules (Fig. S1, Table S1). The critical analysis of the crystal structure of the compound **1**, revels that along with the hydrogen bonding interactions and other prominent supramolecular interactions also have an important contribution to form the overall 3D crystal packing. The dimeric units shown in Fig. 2 form with the individual mononuclear units not only due to the strong intermolecular hydrogen bonding (N4–H4A···O2^a = 2.23 Å and N7–H7NB···N12^a = 2.14 Å) but also the presence of strong π···π interaction between the pyrazine and pyrazole rings with the ring slippage has slip angle of 23.1° and a vertical displacement between the ring centroids of 1.423 Å (centroid separation within Cg5···Cg7^a and Cg5^a···Cg7 = 3.617(15) Å). The individual dimeric units are also interconnected with the adjacent dimeric units with π···π interaction between the other pyrazine and pyrazole rings and form the 1D supramolecular extended structure. The pyrazine and pyrazole ring slippage has slip angle of 14.85° and a vertical displacement between the ring centroids of 1.383 Å (centroid separation within Cg6···Cg8^b and Cg6^b···Cg8 = 3.775(15) Å) (see Fig. 3). Further, 1D chain chains are interlinked through π···π (Cg5···Cg5^c) and C–H···π (C10–H10B···Cg6^d = 2.89 Å) interaction resulting the 2D corrugated sheet like network. The intermolecular π···π slipped-antiparallel stacking interaction of the pyrazole with centroid to centroid (Cg5···Cg5^c) distance 4.167(17) Å, normal distance 3.445(12) Å, horizontal displacement 2.345 Å and torsion angle (Ω1-N6-N6-Ω2) 180° along with the C–H···π (C10–H10B···Cg6^d = 2.89 Å) interaction (see Fig. 4).

3.2. Geometry

The structural parameters along with the crystallographic data of the molecule is listed in Table 1. The computed bond distance and angles are

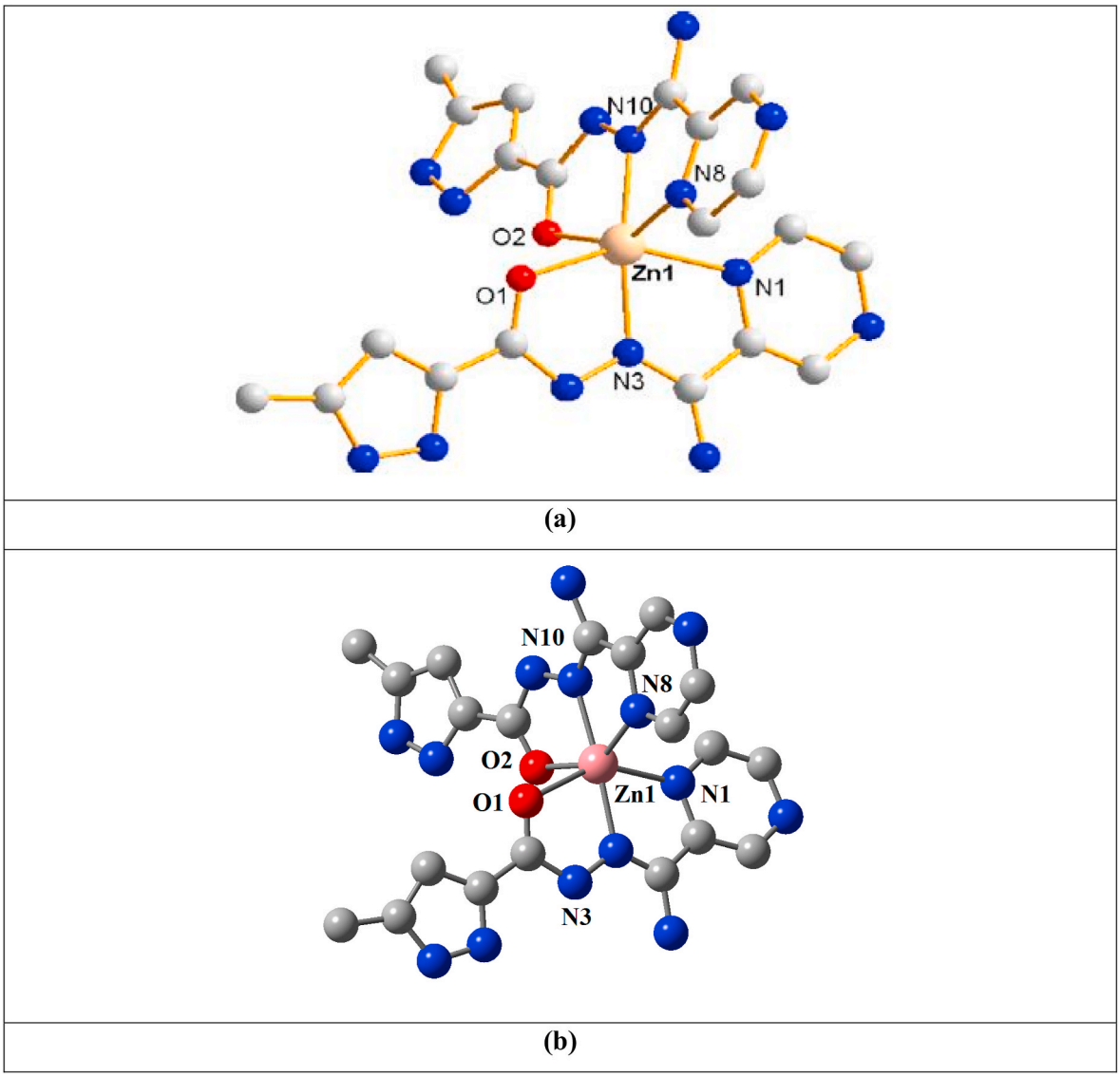

Fig. 5. (a) XRD crystal structure (b) DFT/B3-LYP/6–311++ G(d,p) optimized structure of the Complex **1**. (H atoms were omitted for clarity).

Table 2
FMO energy parameters and global reactivity descriptors of the Complex **1**.

Parameters	Values
HOMO (eV)	−2.807
LUMO (eV)	−2.119
ΔE = (LUMO-HOMO) (eV)	0.688
I = -E(HOMO)(eV)	2.807
A = -E(LUMO) (eV)	2.119
$\chi = (I + A)/2$ (eV)	2.463
$\mu = -\chi$ (eV)	−2.463
$\eta = (I - A)/2$ (eV)	0.344
$S = 1/\eta$ (eV)	2.906
$\omega = \mu^2/2\,\eta$ (eV)	8.817

in good agreement with the experimental geometrical parameters obtained from X-ray crystallography [9]. The DFT optimized structure and the crystal structure from XRD are shown in Fig. 5a, b showing excellent correlation between them. The complex acquires a distorted octahedral geometry. The six donor sites include the four nitrogen atoms and two oxygen atoms of the ligands.

3.3. Frontier molecular orbital (FMO) analysis

The frontier molecular orbital analysis was performed to determine the global reactivity descriptors. The energy gap between frontier molecular orbitals (HOMO and LUMO) of a molecule is an important parameter to predict the stability and reactivity of the system. Various quantum chemical descriptors such as ionization potential (I) and electron affinity (A), global hardness (η), global softness (S), electronegativity (χ), chemical potential (μ) and electrophilicity index (ω) of the molecule is computed and summarized in Table 2. The computed surface plots of HOMO and LUMO is displayed in Fig. 6. The charge density on both the frontier orbitals are majorly localized over the pyrazine part of the complex keeping the pyrazole fragments almost free. The low band gap (0.688 eV) predicts the molecule to be kinetically unstable and chemically reactive through facile charge transfer process. Further, the small hardness value (0.344 eV) of the molecule signifies easy alteration of the electron density and predicts high reactivity of the molecule.

3.4. Electronic spectroscopy

UV–Vis absorption characteristics of the complex was simulated

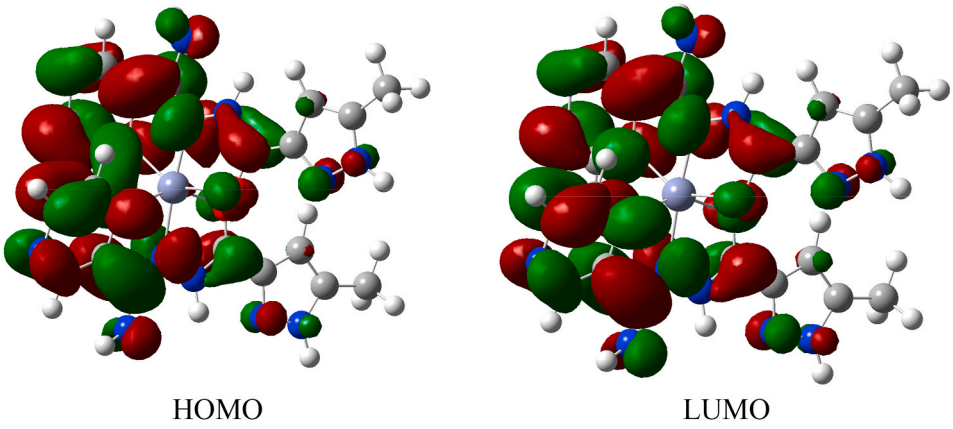

Fig. 6. 3D surface plots of HOMO and LUMO of the Complex **1**.

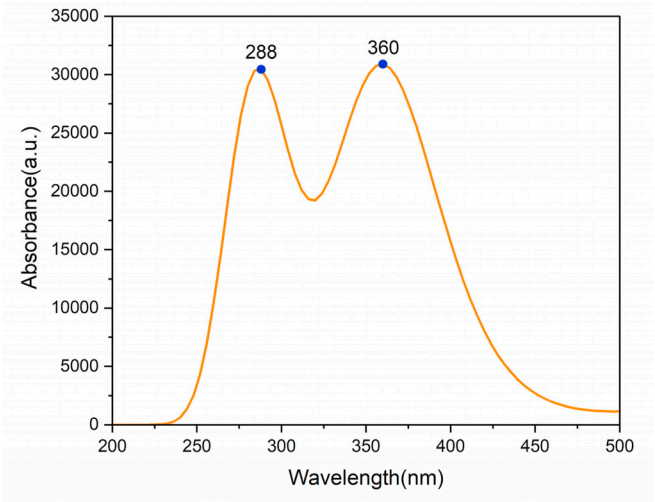

Fig. 7. Simulated absorption spectra in dimethylformamide DMF for complex **1** at TD-M06-CPCM level.

Table 3
Simulated vertical absorptions of the complex (**1**), in dimethylformamide medium at the TD–M06 level.

Electronic transitions	λ_{max} (nm) (TDDFT)	E_{exc}(eV)	f_0	Transition	% C.I.	λ_{max} (nm) (EXP)
$S_0 \rightarrow S_8$	360	3.41	0.16	HOMO→LUMO+1	9.1	470
				HOMO→LUMO+6	3.4	
				HOMO→LUMO+7	2.4	
				HOMO→LUMO+8	4.2	
				HOMO→LUMO+12	5.2	
				HOMO→LUMO+14	2.0	
				HOMO→LUMO+15	11.2	
				HOMO→LUMO+16	5.0	
				HOMO→LUMO+18	2.8	
				HOMO→LUMO+19	7.3	
				HOMO→LUMO+21	10.7	
				HOMO→LUMO+22	4.6	
				HOMO→LUMO+23	2.4	
				HOMO→LUMO+27	2.7	
$S_0 \rightarrow S_{17}$	288 (TDDFT)	4.31	0.39	HOMO-8→LUMO	3.7	352
				HOMO-4→LUMO	8.8	
				HOMO-2→LUMO	50.1	
				HOMO→LUMO+7	5.3	
				HOMO→LUMO+9	2.8	
				HOMO→LUMO+17	2.6	
				HOMO→LUMO+28	2.5	

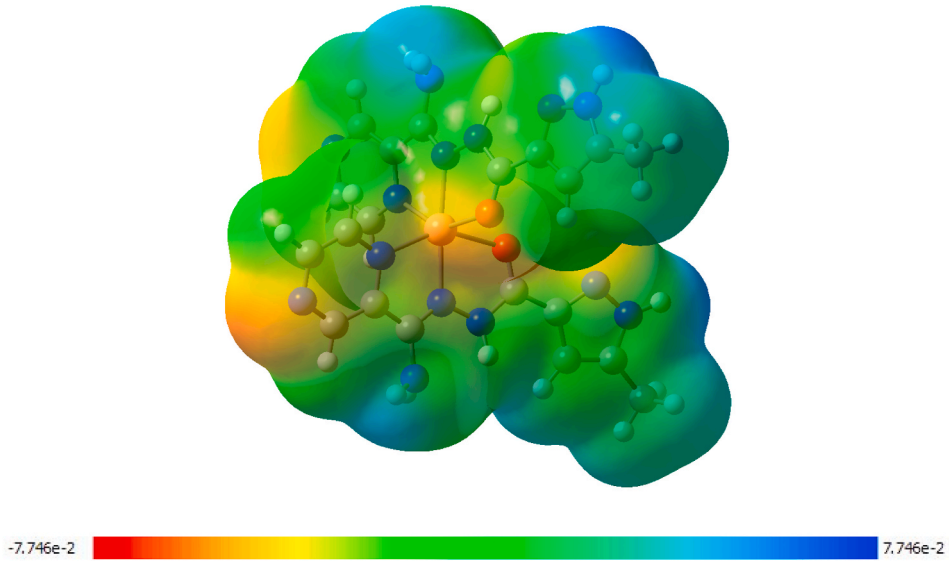

Fig. 8. Molecular electrostatic potential map of the Complex **1**.

using TDDFT approach in DMF solvent. Using the optimized ground state structure, the singlet→singlet vertical transitions are calculated by TD-M06/6-31 + G(d)-LANL2DZ level using conductor like polarizable continuum (CPCM) solvation model. The predicted absorption spectrum is shown in Fig. 7. The graph shows two intense transitions at 288 and 360 nm. The 288 nm transition is attributed due to intra ligand π→π* and n→π* transitions. While the transition at 360 nm is due to the MLCT band [9]. The absorption data containing λ_{max}, Excitation energy, oscillator strength, assignment of transitions and configuration interaction (CI) are listed in Table 3. The experimental λ_{max} taken from Ref. [9] is also shown for comparison. The MLCT transition at 360 nm is associated with the transition of electron from HOMO and various lower HOMO to LUMO and various higher LUMO orbitals. While the π→π* and n→π* transition at 288 nm involve the electron transfer from HOMO to various higher LUMO orbitals.

3.5. Molecular electrostatic potential (MEP)

The electrostatic potential of a molecular entity is a valuable tool to predict electrophilic and nuleophilic sites within the molecule. The propensity of formation of various types of intermolecular interactions for example, hydrogen bonding, drug-receptor interaction, enzyme-substrate interactions etc. is majorly based on the electrostatic potential of the molecule [12]. The MEP of the metal complex is calculated using electron density of the optimized structure and displayed in Fig. 8. The 3D map highlights the electron density in terms of different colour in increasing order blue < green < yellow < orange < red. The figure indicates the presence of high electron density or negative charge around the donor oxygen atoms near the metal centre and nitrogen atoms of the pyrazine rings (orange-red colored surface). The area around the pyrazole group displays greenish blue colour indicating electron deficiency. Thus, the electrophilic reactivity of the complex will be centered around the metal centre and pyrazine rings whereas nucleophilic reactivity around the pyrazole rings of the molecule.

3.6. Hirshfeld surface analysis

The Hirshfeld surfaces of the compound mapped in terms of *d*norm, curvedness and shape index are shown in Fig. 9a–d. The *d*norm surface represents the normalized contact distance. Several red spots in the *d*norm surface in various size and intensities indicates the atoms present in close proximity to the outer side of Hirshfeld surface. The most prominent red spots are arising due to donor-acceptor interactions comprising of N–H···N and O–H···N hydrogen bonding interactions. The white and blue surfaces indicate atoms with medium proximity and large distance respectively from the Hirshfeld surface. The intermolecular interactions involving hydrogen bonds in the molecule are depicted in Fig. 9e. The figure shows that O12–H12···N2 and O12–H12···C2 hydrogen bond between O12 of solvent methanol and N2 and C2 of pyrazine ring respectively. Another hydrogen bond interaction of type N7–H7B···N12 between N12 atom of pyrazole with N7–H7B of amine group. The shape index and curvedness determine the shape and surface area of the molecule. The shape index is a key parameter in understanding the presence of π···π stacking interactions in the packing modes of the crystal [13]. The shape index surface shows a few adjacent red and blue triangles (encircled region) indicating the presence of adjacent concave and convex region. This implies that the molecular crystal is stabilized with week π···π stacking interactions. The donor-acceptor interactions between two molecules are displayed in shape index by colour coded bumps and hollows. The blue region represents bump complement to the donor while red hollow region corresponds to the acceptor. Similar type of curvedness and shape index surfaces are reported by previous researchers [14,15]. Further the curvedness map supports the findings of shape index. The presence of flat surface patches in the curvedness map clearly tells that the crystal is packed with weak π … π stacking interactions which is clearly visible in the circled region. The dark blue edges are linked to high curvedness and green flat edges around the pyrazole ring corresponds to low curvedness advocating for presence of π … π stacking interactions.

The two-dimensional fingerprint plots (Fig. 10) of the major contacts are determined to quantify the intermolecular interactions. The molecular crystal is mostly packed with O···H and N···H contacts as major interactions contributing about 40.9 % and 11.6 % respectively to the overall crystal packing. Both O···H and N···H contacts in the FP plots are visible with their signature symmetrical sharp spikes. This special feature of O···H and N···H contacts signify presence of hydrogen bonding interactions in the crystal [16]. The *de* + *di* of O···H and N···H contacts are found to be at 1.7 and 1.8 Å respectively indicating their strong nature of interaction. Another important contact playing key role in framing the supramolecular crystal is H···H contact with 27.1 % contribution displaying a pair of small peaks at *de* + *di* of 2.3 Å. Additionally, C···O and C···H contacts contribute 5.5 % and 4.9 % respectively in stabilizing the molecular crystal. The sharpest point in C···O and C···H contacts featured a close contact of *de* + *di* value at 2.9 and 2.8 Å respectively. The C···H contacts display characteristics wing feature with bow-tie pattern confirming the presence of weak π···π stacking

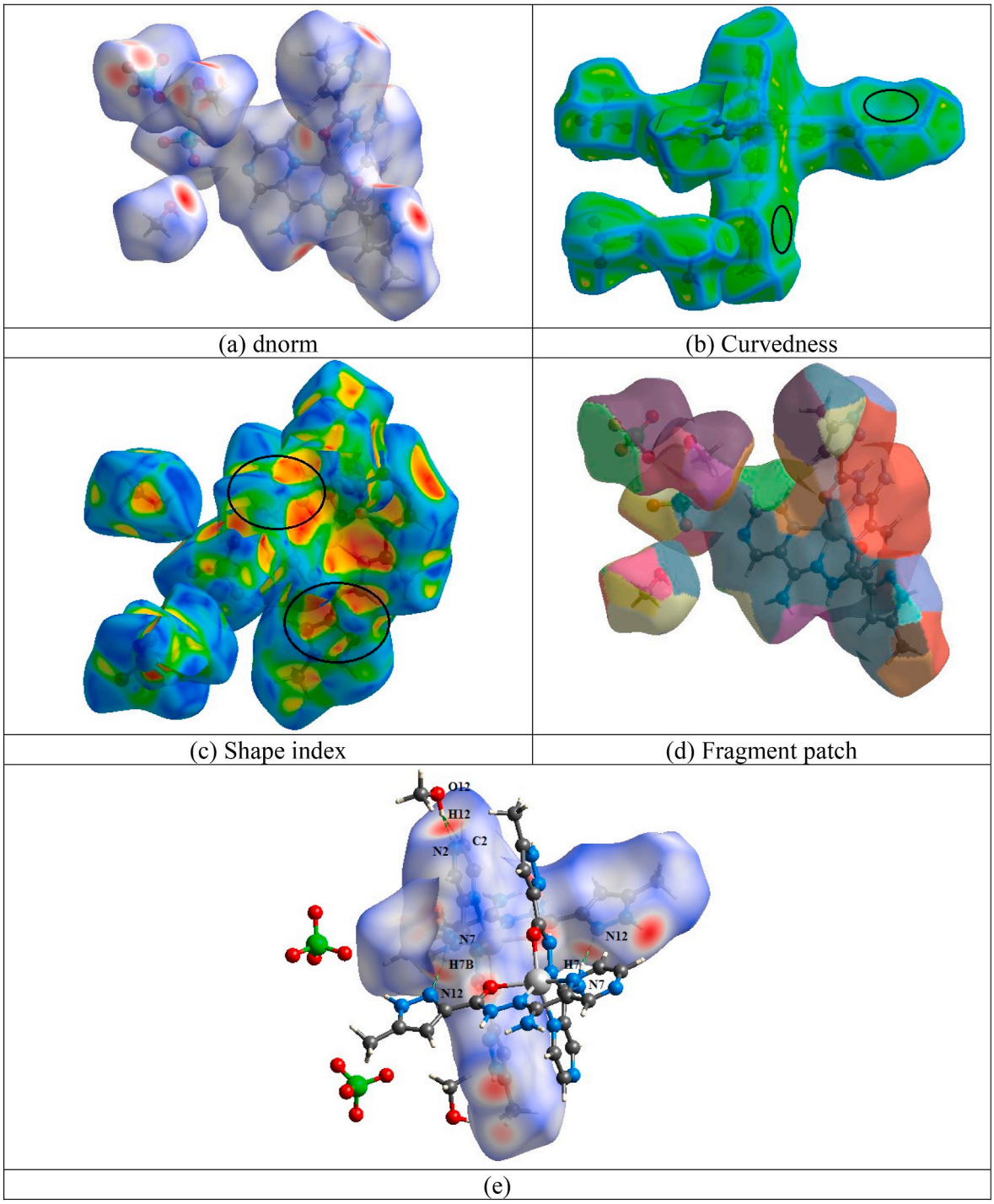

Fig. 9. Hirshfeld surfaces mapped over (a) d_{norm}, (b) curvedness(c) shape index and (d) Fragment patch (e) Intermolecular interaction showing H-bonds.

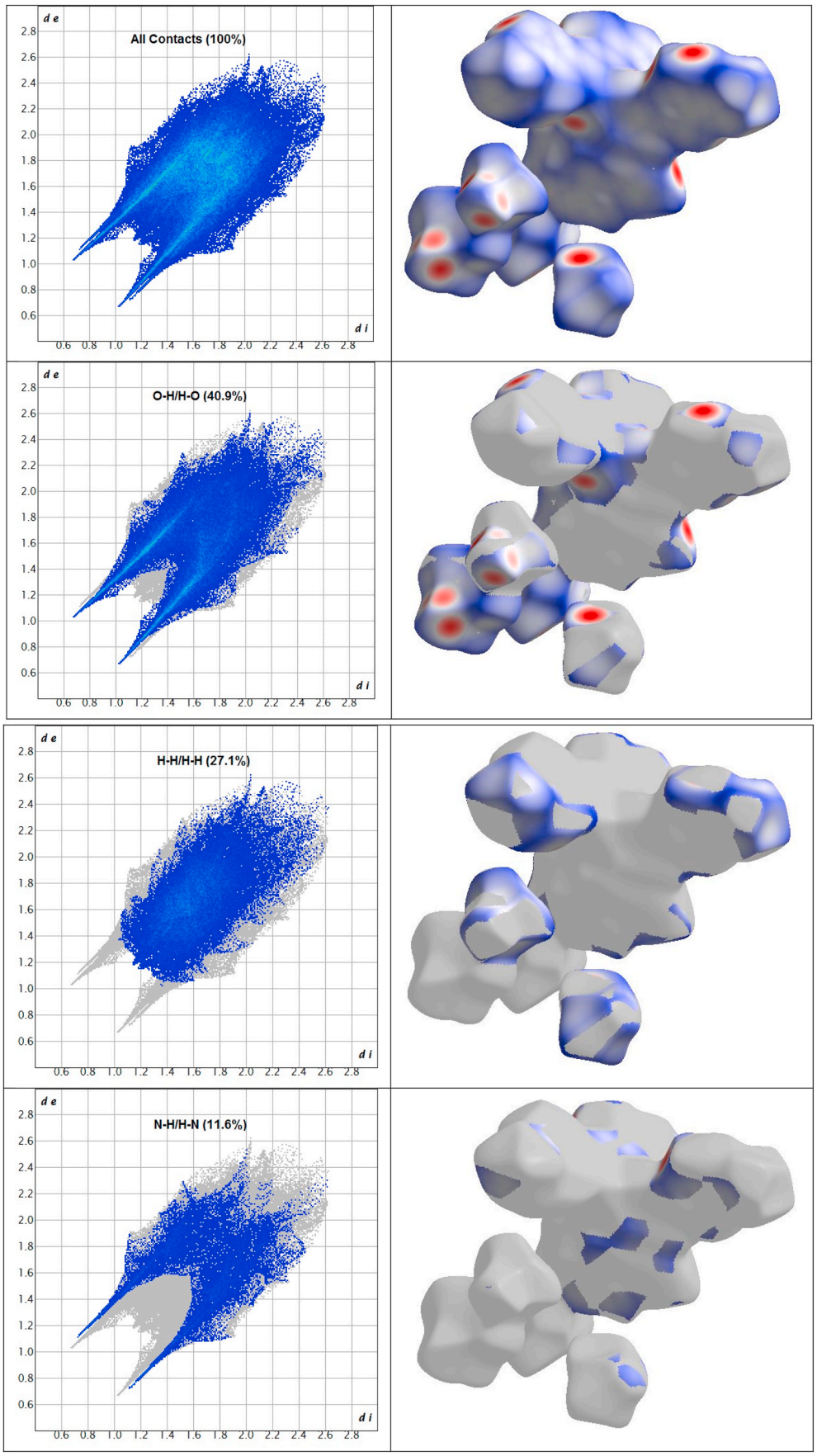

Fig. 10. Two-dimensional fingerprint plot of the complex showing the contributions of individual interactions: Outline of the full fingerprint is shown in grey. Surfaces to the right highlight the relevant surface patches associated with the specific contacts with dnorm mapped.

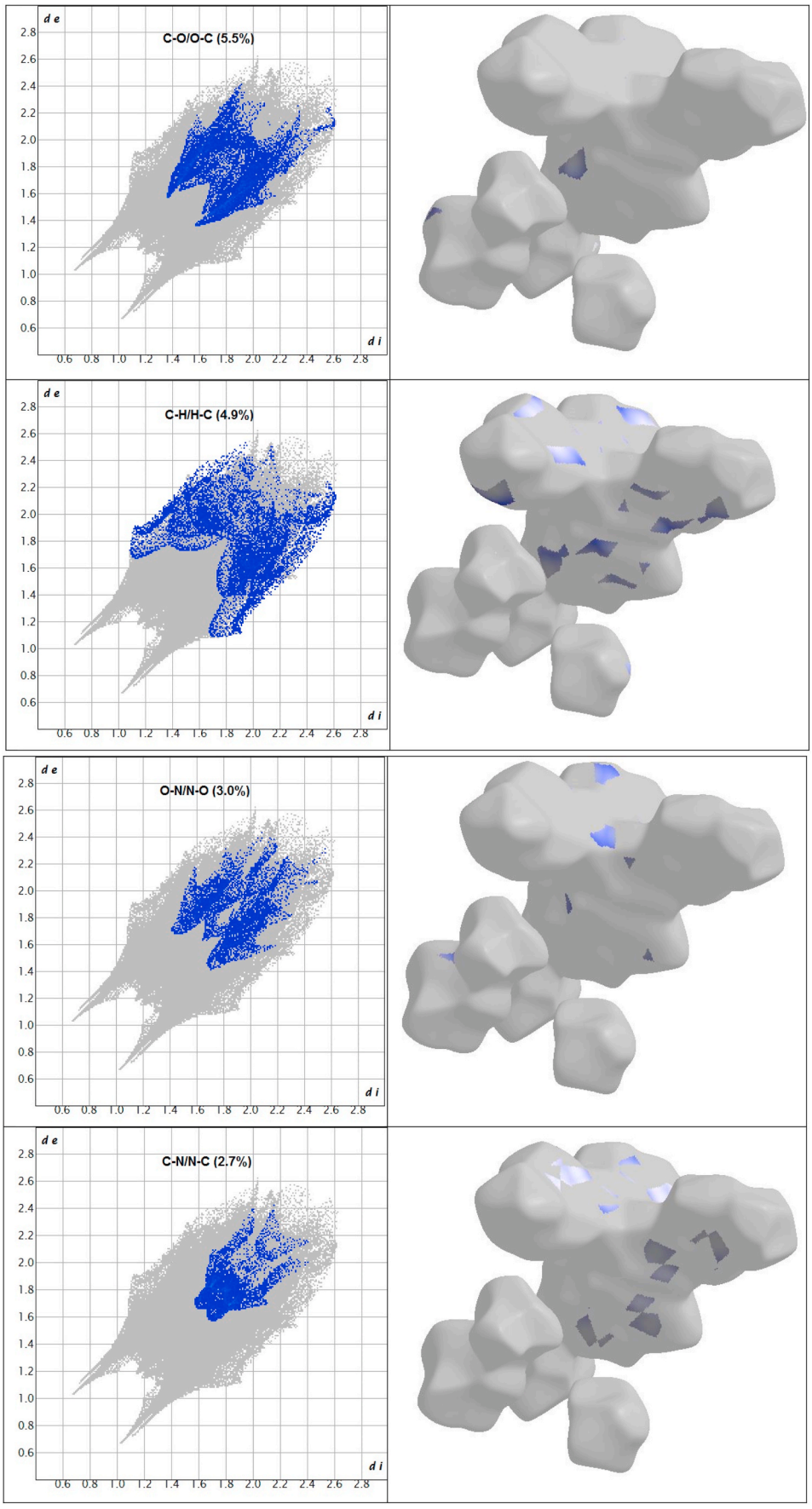

Fig. 10. (*continued*).

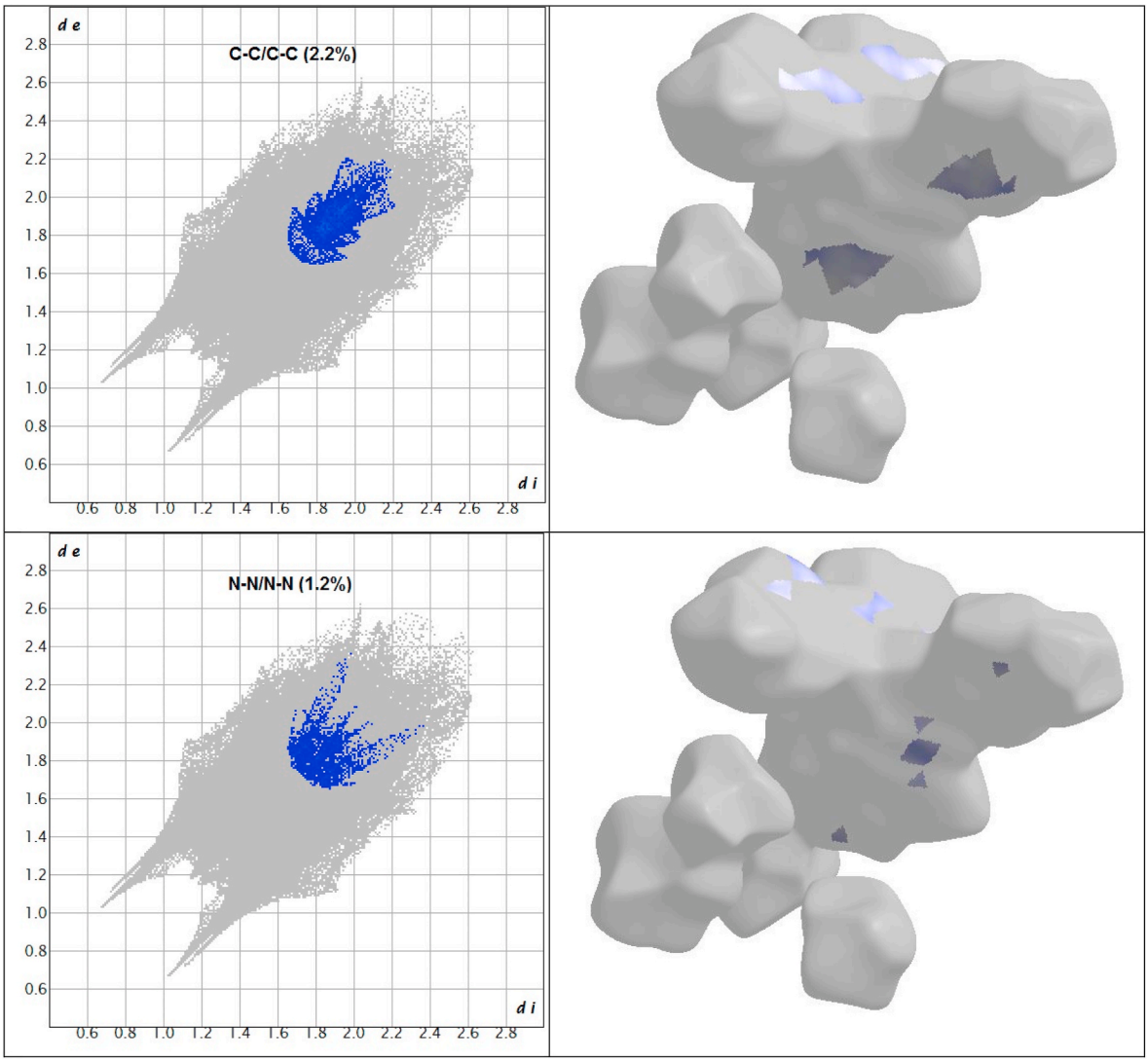

Fig. 10. (*continued*).

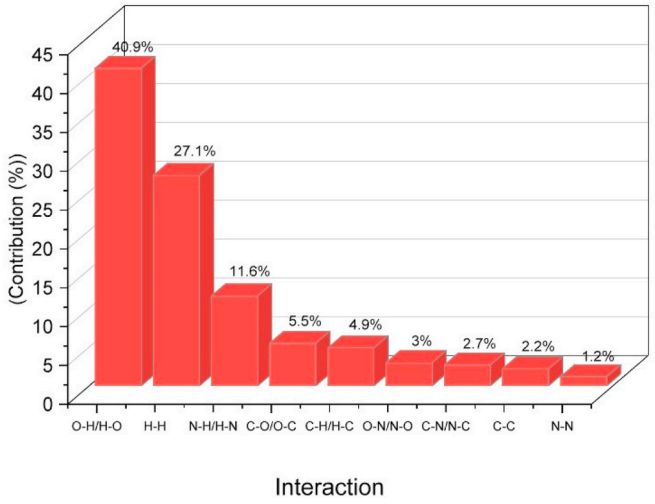

Fig. 11. Relative contributions of various interactions to the Hirshfeld surface of complex **1**.

interactions and C–H … π interaction in the crystal [8,17,18]. Other interactions with minor contribution in the crystal packing are O···N, C···C, C···N, and N···N. Fig. 11 summarizes the relative contributions of various interactions to the Hirshfeld surface.

4. Conclusion

The supramolecular interactions play a crucial role in assembling the molecules into an organized framework. The solid-state structure illustrates how intermolecular π···π and C–H···π interactions lead to the creation of a 1D network. The value of the Hirshfeld analysis in comprehending the intricate interactions that take place in crystallized solids is highlighted in this work. Hirshfeld surface analysis, a revolutionary approach in crystal structure prediction, allows for considerably greater inspection by exhibiting all intermolecular interactions by quantifying them in a 2D fingerprint plot within the crystal. This research supports the crucial part that π···π stacking and C–H···π interactions play in the crystal structure and molecular cluster formation. FMO analysis predicts the molecule to be kinetically unstable and chemically reactive through facile charge transfer process. MEP analysis clearly shows the electrophilic reactivity of the complex will be centered around the metal centre and pyrazine rings whereas nucleophilic reactivity around the pyrazole rings of the molecule.

Conflict of interests

The authors declare that they have no conflict of interests.

CRediT authorship contribution statement

Suranjana Chatterjee: Conceptualization, Data curation. **Mohd Afzal:** Funding acquisition, Investigation. **Pulak Chandra Mandal:** Formal analysis, Software. **Ritwik Modak:** Validation, Visualization. **Mridula Guin:** Methodology, Software, Writing – original draft. **Saugata Konar:** Supervision, Writing – original draft, Writing – review & editing.

Declaration of competing interest

The authors declare that they have no known competing financial interests or personal relationships that could have appeared to influence the work reported in this paper.

Acknowledgments

The author Mohd Afzal extends his appreciation to the "Researchers Supporting Project number (RSPD2024R979)", King Saud University, Riyadh, Saudi Arabia for financial assistance.

Appendix A. Supplementary data

Supplementary data to this article can be found online at https://doi.org/10.1016/j.jics.2024.101275.

References

[1] C. Hopa, Ni(II) and Co(II) acetato complexes of pyrazole-pyridine based ligand: synthesis, structure and thermal decomposition, J. Struct. Chem. 64 (2023) 954–961, https://doi.org/10.1134/S002247662305013X.

[2] S. Konar, A. Jana, K. Das, S. Ray, S. Chatterjee, S.K. Kar, Complexes of a functionally modified pyrazole derived ligand - mononuclear zinc(II), dinuclear nickel(II) and a rare pentanuclear cadmium(II) complex with a TBP core and their photoluminescence studies, Polyhedron 47 (2012) 143–150, https://doi.org/10.1016/j.poly.2012.07.080.

[3] S.D. Kanmazalp, N. Dege, I.O. Ilhan, N. Akin, Crystal structure and Hirshfeld surface analysis of 3,5-Bis(4-methoxyphenyl)-4,5-dihydro-1H-Pyrazole-1-Carbothioamide, J. Struct. Chem. 61 (2020) 126–132, https://doi.org/10.1134/S002247662001014X.

[4] J. Rajamoni, S. Kandasamy, Structural features and N-H…O and O-H…O hydrogen-bonded supramolecular frameworks in 2-methylanilinium hydrogen DL-malate hydrate, 4-methoxyanilinium and 4-methylanilinium hydrogen DL-malate salts, Struct. Chem. 31 (2020) 917–925, https://doi.org/10.1007/s11224-019-01441-7.

[5] S. Pramanik, S. Konar, K. Chakraborty, T. Pal, S. Das, S. Chatterjee, M. Dolai, S. Pathak, Investigation of electrical conductance properties, non-covalent interactions and TDDFT calculation of a newly synthesized copper(II) metal complex, J. Mol. Struct. 1206 (2020) 127663, https://doi.org/10.1016/j.molstruc.2019.127663.

[6] Y. Wang, C.S. Zhao, Synthesis, crystal structure and DFT study of ethyl 5-(trimethylsilyl)-1-1H-Pyrazole-3-Carboxylate, J. Struct. Chem. 64 (2023) 603–617, https://doi.org/10.1134/S002247662304008X, 2020.

[7] Ö. Tamer, B. Sarıboğa, İ. Uçar, A combined crystallographic, spectroscopic, antimicrobial, and computational study of novel dipicolinate copper(II) complex with 2-(2-hydroxyethyl)pyridine, Struct. Chem. 23 (2012) 659–670, https://doi.org/10.1007/s11224-011-9910-0.

[8] M. Guin, S. Halder, S. Chatterjee, S. Konar, Synthesis, X-ray crystal structure of Cu (II) 1D coordination Polymer: in View of Hirshfeld surface, FMO, Molecular electrostatic potential (MEP) and Natural Bond orbital (NBO) analyses, J. Mol. Struct. 1270 (2022) 133949, https://doi.org/10.1016/j.molstruc.2022.133949.

[9] S. Konar, A. Jana, K. Das, S. Ray, J.A. Golen, A.L. Rheingold, S.K. Kar, A rare pentanuclear cadmium(II) complex and two new mononuclear zinc(II) complexes of pyrazole derived ditopic ligands – synthesis, crystal structuresand spectral studies, Inorg. Chim. Acta. 397 (2013) 144–151, https://doi.org/10.1016/j.ica.2012.12.003.

[10] Gaussian 16, Revision C.01, Frisch M J, Trucks G W, Schlegel H B, Scuseria G E, Robb M A, Cheeseman J R, Scalmani G, Barone V, Petersson G A, Nakatsuji H, Li X, Caricato M, Marenich A V, Bloino J, Janesko B G, Gomperts R, Mennucci B, Hratchian H P, Ortiz J V, Izmaylov A F, Sonnenberg J L, Williams-Young D, Ding F, Lipparini F, Egidi F, Goings J, Peng B, Petrone A, Henderson T, Ranasinghe D, Zakrzewski V G, Gao J, Rega N, Zheng G, Liang W, Hada M, Ehara M, Toyota K, Fukuda R, Hasegawa J, Ishida M, Nakajima T, Honda Y, Kitao O, Nakai H, Vreven T, Throssell K, Montgomery J A, Peralta Jr J E, Ogliaro F, Bearpark M J, Heyd J J, Brothers E N, Kudin K N, Staroverov V N, Keith T A, Kobayashi R, Normand J, Raghavachari K, Rendell A P, Burant J C, Iyengar S S, Tomasi J, Cossi M, Millam J M, Klene M, Adamo C, Cammi R, Ochterski J W, Martin R L, Morokuma K, Farkas O, Foresman J B, Fox D. J. (2016) Gaussian, Inc., Wallingford CT.

[11] M.J. Turner, J.J. McKinnon, S.K. Wolff, D.J. Grimwood, P.R. Spackman, D. Jayatilaka, M.A. Spackman, CrystalExplorer17, The University of Western Australia, 2017.

[12] S. Lakshminarayanan, V. Jeyasingh, K. Murugesan, N. Selvapalam, G. Dass, Molecular electrostatic potential (MEP) surface analysis of chemo sensors: an extra supporting hand for strength, selectivity & non-traditional interactions, J. Photochem. Photobiol. 6 (2021) 100022, https://doi.org/10.1016/j.jpap.2021.100022.

[13] M.A. Spackman, J. Dylan, Hirshfeld surface analysis, CrystEngComm 11 (2009) 19–32, https://doi.org/10.1039/B818330A.

[14] A. Saeed, S. Ashraf, U. Flörke, Z.Y.D. Espinoza, M.F. Erben, H. Pérez, Supramolecular self-assembly of a coumarine-based acylthiourea synthon directed by π-stacking interactions: crystal structure and Hirshfeld surface analysis, J. Mol. Struct. 1111 (2016) 76–83, https://doi.org/10.1016/j.molstruc.2016.01.074.

[15] Y. Yang, C. Feng, Y. Jiang, D. Du, H. Zhao, G. Zhang, Y. Wang, Q. Zhao, Synthesis, crystal structure, Hirshfeld surface analysis and electrochemiluminescence property of A 2D Ag(I) coordination polymer, J. Mol. Struct. 1292 (2023) 136145, https://doi.org/10.1016/j.molstruc.2023.136145.

[16] L.H. Al-Wahaibi, J. Joubert, O. Blacque, N.H. Al-Shaalan, A.A. El -Emam, Crystal structure, Hirshfeld surface analysis and DFT studies of 5-(adamantan-1-yl)-3-[(4-chlorobenzyl)sulfanyl]-4-methyl-4H-1,2,4-triazole, a potential 11β-HSD1 inhibitor, Sci. Rep. 9 (2019) 19745, https://doi.org/10.1038/s41598-019-56331-z.

[17] A. De, M.A. Kathait, P. Jain, M. Guin, DFT investigation, Hirshfield analysis and molecular docking of Cu (II) complex of O-Vanillin based ligand, ChemistrySelect 7 (42) (2022) e202202884, https://doi.org/10.1002/slct.202202884.

[18] S.J. Munshi, M. Guin, S. Kundu, S.B. Kumar, Synthesis, Structures and Hirshfeld surface analysis of Ni(II) and Co(III) complexes with N2O donor Schiff base ligand, J. Indian Chem. Soc. 98 (2021) 100080, https://doi.org/10.1016/j.jics.2021.100080.